

Clinically Approved MRI Contrast Agents as Imaging Labels for a Porous Iron-Based MOF Nanocarrier: A Systematic Investigation in a Clinical MRI Setting

Konstantin Böll, Andreas Zimpel, Olaf Dietrich, Stefan Wuttke,* and Michael Peller*

Metal-organic framework nanoparticles (MOF NPs) are a promising class of NP systems that offer versatile and tunable properties. Creating a magnetic resonance imaging (MRI)-MOF NP platform as a basis for a theranostic drug delivery system is considered an auspicious approach, as MRI is a routinely used clinical method allowing real-time imaging. So far clinically approved MRI contrast agents (CAs) have not been investigated systematically for the visualization of loading and release from MOF NPs. Here, loading and release of six clinically approved CAs from the MOF MIL-100(Fe) are investigated in a clinical MRI setting. Standard procedures, beginning with sample preparation up to MRI methods, are established for that purpose. Results are reproduced and verified by Inductively Coupled Plasma Atomic Emission Spectrometry (ICP-AES) and thiocyanate testing. The macrocyclic CA gadoterate meglumine is identified as the best CA candidate for labeling MIL-100(Fe). The CA is successfully loaded after 1 h, and also effectively released within the first hour. The MR-active CA and iron residuals in supernatants are differentiable based on MRI only and concentrations can be successfully calculated. The presented systematic approach suggests procedures and MRI-methodology that can be used as blueprint strategy when labeling porous NPs with clinically approved MRI CAs.

1. Introduction

Biomedical imaging labels in combination with nanocarriers allow for a real-time tracing of that nanocarrier for the assessment of the biodistribution as well as an understanding of the targeting and delivery process. One of the most promising aspects of combining therapy and imaging is to optimize the delivery of the drug for a specific patient.^[1] A long-standing challenge towards this goal is the question whether the drug has been released and delivered to the targeted tissue or cells.^[2] The mere accumulation of the nanocarrier in the target tissue does not necessarily lead to a higher bioavailability of the drug.^[2,3]

A large library of different theranostic nanocarrier systems has been synthesized in order to address this challenge, but unfortunately these efforts did not result in a comparable number of clinically applicable products.^[4] As an improvement of this situation, new promising nanocarrier material systems could be tested in

conditions that are as close as possible to their intended later clinical application. This means naturally that imaging labels should be used which can be visualized with standard clinical imaging methods.

Magnetic resonance imaging (MRI) is a widespread, very versatile standard clinical imaging method using the nuclear magnetic moment of proton spins predominantly of water in the human body. It is non-invasive, does not require ionizing radiation, and allows for a mapping of the internal structure and certain aspects of function within the body. Additionally, MRI offers a variety of approved imaging labels (contrast agents—CA) and a broad spectrum of signal forming mechanisms, in principle allowing for a tuned visualization of nanocarriers.^[5] Furthermore, magnetic resonance is a standard analysis method used in basic, preclinical, and clinical research and therefore can be expected to simplify translational approach for nanocarrier development.


The loading and release of an MRI imaging label such as MRI-CA could allow for the visualization of a successful delivery to the target site and a release of the CA at the same time.^[6] However, to the best knowledge of the authors, there are no studies comparing the loading/release of different clinically used MRI-CAs from porous nanoparticles (NPs) in a systematic way. Additionally, the quantification of therapeutic drug concentration, in the

K. Böll, Dr. O. Dietrich, Dr. M. Peller
Department of Radiology
University Hospital, LMU Munich
81377 Munich, Germany
E-mail: michael.peller@med.uni-muenchen.de

Dr. A. Zimpel, Prof. S. Wuttke
Department of Chemistry and Center for NanoScience (CeNS)
LMU Munich
81377 Munich, Germany
E-mail: Stefan.Wuttke@cup.lmu.de

Prof. S. Wuttke
BCMaterials, Basque Center for Materials
UPV/EHU Science Park
48940 Leioa, Spain

Prof. S. Wuttke
Ikerbasque
Basque Foundation for Science
48013 Bilbao, Spain

 The ORCID identification number(s) for the author(s) of this article can be found under <https://doi.org/10.1002/adtp.201900126>

© 2019 The Authors. Published by WILEY-VCH Verlag GmbH & Co. KGaA, Weinheim. This is an open access article under the terms of the Creative Commons Attribution License, which permits use, distribution and reproduction in any medium, provided the original work is properly cited.

DOI: 10.1002/adtp.201900126

sense of chemodosimetry, may be envisioned if a correlation of CA and drug release is possible. The principal feasibility has already been shown using thermosensitive liposomes loaded with doxorubicin and MRI CA.^[6]

Since porous hybrid NPs provide ideal scaffolds for the combination of different functional units, they are considered as promising nanocarrier systems in the field of nanomedicine.^[1,7] In this respect, metal-organic framework (MOF) NPs are one of the most promising nanocarrier systems that offer versatile and tunable properties.^[8] Due to their hybrid nature and high porosity, MOF NPs are considered as ideal host systems for the controlled delivery of active molecules and/or as a platform for medical imaging. While their limited apertures inhibit the loading of large molecules or proteins, MOF NPs have been shown to be efficient nanocarriers using different pharmaceutical agents.^[9] In addition, MOFs are biodegradable and they can be constructed from biocompatible building blocks implying a low toxicology.^[8,10] For the study presented here, MIL-100(Fe) NPs (MIL: Materials of Institute Lavoisier) were chosen as a model system because they are considered the most suitable MOF nanocarrier systems for clinical purposes.^[8–11]

To further enhance the clinical applicability of this study, clinically approved, unmodified MRI CAs were used as imaging labels for MIL-100(Fe) NPs and the CA loading and release behavior was systematically investigated in a clinical MRI setting. Different CAs with varying chemical and physical properties are available for clinical MRI and are potentially usable as imaging labels.^[5,12] Currently, Gd-based CAs are the de facto standard class of MRI CAs^[12] and for that reason, this study focused on Gd-based CAs only. Although being used for decades, two classes out of three, linear ionic and linear nonionic clinically approved Gd-based CA, are currently under discussion for safety issues in specific patients^[13] and only the third class, consisting of three macrocyclic Gd chelates, is left in clinical routine.^[12] However, as the CA-guest/MOF-host interactions are strongly influenced by the individual chemical nature of the CA, the whole spectrum of clinically approved Gd-based CAs, including those, which are currently under safety discussion, was investigated. A set of six Gd-based CAs was selected for this study—two macrocyclic Gd chelates (Dotarem/gadoterate meglumine; Gadovist/gadobutrol), three linear ionic Gd chelates (Magnevist/gadopentetate dimeglumine; MultiHance/gadobenate dimeglumine; Primovist/gadoxetic acid disodium) and one linear nonionic Gd chelate (Omniscan/gadodiamide; see also Supporting Information).

The research presented here aims to address the question how loading and release of different clinically approved MRI CAs by porous NPs can be systematically investigated in a clinical MRI setting. By investigating approved MRI-CAs and by choosing a clinical MRI system, relevant factors influencing the visualization for a potential clinical use were already an integrative part of this study. One aim of this study was to find applicable MRI methods and test their precision. Finally, by choosing one of the most studied and promising MOF drug delivery systems, MIL-100(Fe), the door is being opened to use these NPs as a future theranostic nanocarrier system as well as adding a new concept for labeling MOF drug delivery systems.

2. Results and Discussion

Several clinically approved CA candidates are potentially suitable for loading into MIL-100(Fe). The first step was to identify the most suitable candidate from several clinically approved MRI-CAs and to develop a suitable experimental procedure for the selection. The challenge here was that MIL-100(Fe) NPs^[11,14] and naturally the MRI-CAs are both MR-active and it is not straightforward to assess loading and release processes in real-time without detailed knowledge of these processes. The separation of the two contributions is impeded because all these processes can affect the MRI signal in a similar way by changing the relaxation times T_1 and T_2 of the water protons (or their reciprocals, i.e., the relaxation rates R_1 and R_2). In order to facilitate an unambiguous interpretation of loading and release processes, only supernatants after removing the NPs were used in the selection process and also in succeeding experiments.

The MIL-100(Fe) NPs were prepared in a procedure according to literature.^[11,15] The detailed characterization of those NPs can be found in Figures S1–S5, Supporting Information. All results confirm that the NPs are similar to those reported in literature.^[11,15]

2.1. Selecting a Suitable CA for Loading and Development of Experimental Procedure

Six clinically approved gadolinium-based CAs (Dotarem, Magnevist, Multihance, Primovist, Gadovist, and Omniscan) were tested applying the same loading procedure for each CA. The NPs were incubated for 1 h in 1.25 mM aqueous solution of each CA. A successful loading of the NPs with the CA was expected to reduce the concentration of free CA in the solution and, thus, in the supernatant after removal of the NPs. NP pellets gained when preparing the supernatant samples were stored for later analysis as described below.

In MRI, a decreasing CA concentration will result in decreasing R_1 and R_2 values. Thus, a successful loading of a CA to the NPs was expected to result in decreasing relaxation rates in the supernatant when compared to those relaxation rates before starting the loading procedure. In case of unsuccessful loading, no or only minor changes of relaxation rates should be found. **Figure 1** shows R_1 values (the corresponding results for R_2 are presented in Figure S6, Supporting Information) of the aqueous supernatants of all six CAs used during incubation of MIL-100(Fe) NPs. For comparison, the figure shows the relaxation rates of the respective aqueous solutions containing free CA with the concentration prepared before the loading procedure. Two types of results were identified. In one group, the anticipated relaxation rate decrease was detected when using Dotarem, Magnevist, Multihance, and Primovist. This was interpreted as successful loading to NPs. Contrary to this decrease of the relaxation rate, an increase of R_1 and R_2 was observed in a second group using Gadovist and Omniscan. Because of this unexpected behavior and for verification, the whole process was repeated using three individually prepared sets of samples that were measured separately. This was also done to test the reproducibility of sample preparation and MRI methods. Repeating the experiments showed highly reproducible results (Figures 1 and Figure S6,

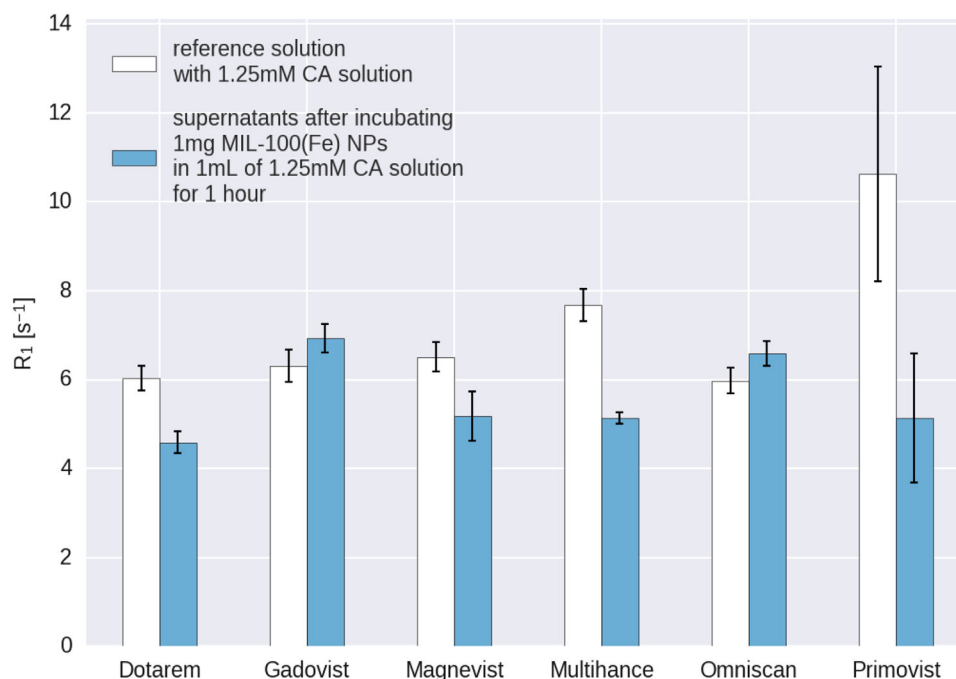


Figure 1. MR measurements of reference solutions (white) and supernatants after incubation of 1 mg MIL-100(Fe) NPs in 1.25 mM aqueous solution of CA (blue). Three individually prepared sets of samples with each CA were measured. Each error bar shown denotes the standard deviation of the determined relaxation rate R_1 mean values for the three individually prepared and measured samples (corresponding R_2 mean values shown in Figure S6, Supporting Information).

Supporting Information). The finding of these two groups indicates that other MR-active, competing processes were present in the second group besides the anticipated effects related to loading in the first group. Such competing processes could potentially be caused by decomposing Fe-based MOF NPs and concomitantly increasing iron content in the supernatant, which is itself also MR-active. Please note that results using Primovist were less reproducible, compared to the other CAs, although samples were measured together with those of other CAs. Thus, varying results were not related to MRI methods and were assumed to be caused by additional unknown processes of the sample.

Two additional analysis methods were applied for further verification of the assumption that the expected relaxation rate reduction seen in the first group is related to a CA-loading process and to further look into the unexpected results of the second group. NP pellets that were collected when preparing the supernatants were analyzed by Inductively Coupled Plasma Atomic Emission Spectrometry (ICP-AES), determining the ratio of gadolinium to iron content in each pellet. Additionally, the iron content in the supernatants was determined using a thiocyanate test with the idea to identify NP decomposition. The reduced Gd/Fe ratio in the pellets (**Figure 2**) indicates a lower uptake of Gadovist and Omniscan compared to the other four CAs. Additionally, using Gadovist and Omniscan also leads to an increased iron concentration in the supernatants suggesting a decomposition of the NPs which could explain the unexpected, increasing relaxation rates. The other four CAs showed desirable results and were considered promising for further testing.

The lower CA uptake and the higher release of iron ions into the solution in group 2 with Gadovist and Omniscan led to their

exclusion for further investigations considering them as unsuitable. The results for the loading process with Primovist were less easily reproducible than the others and thus Primovist was also excluded. Of the remaining three CAs, Dotarem, Magnevist, and Multihance, Dotarem was the only macrocyclic CA. Macrocyclic Gd-based CAs are currently considered to be safer for clinical application inside humans.^[12] Thus, Dotarem was considered the most promising candidate for loading into MIL-100(Fe) and the most suitable CA for a potential later clinical use. Due to the high experimental efforts, the following investigations focused on using Dotarem only. The question why the other CAs were less suitable or led to unexpected results was considered beyond the scope of this work.

2.2. Testing CA Loading of Dotarem in Water and Diverse Buffers

For further optimization of the loading process and also to test the sensitivity of the process to varying chemical environments, diverse buffers were tested. **Figure 3** and **Figure S7**, Supporting Information, show the relaxation rates of the supernatants after applying the same loading and preparation processes with the same Dotarem concentration (2 mM) but using water and six different physiological buffers. These buffers are frequently used in biology, pharmacy, and biomedicine. Besides bidistilled water, three representatives of the Good's-buffers (MES, HEPES, and TRIS) were chosen because of their buffer capacity from slightly acidic (MES) to neutral (HEPES) and slightly basic (TRIS) pH. To mimic more acidic conditions present, for example, in human

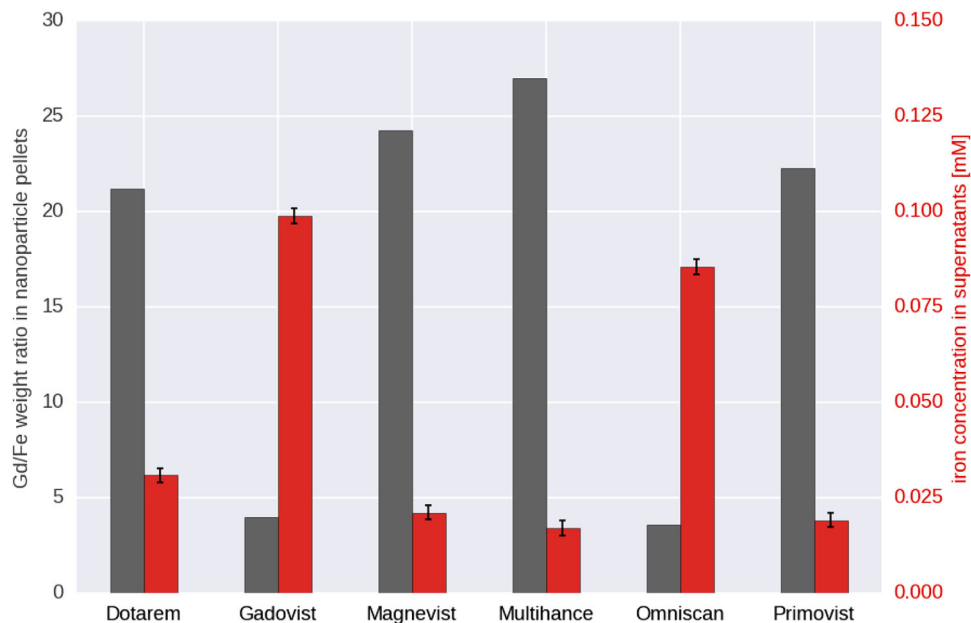


Figure 2. ICP-AES measurements of removed MIL-100(Fe) NP pellets after incubation in the different CAs (gray) and thiocyanate test of the remaining supernatants (red). The Gd/Fe ratio in the removed NP pellets (gray), determined via ICP-AES, for the CAs Gadovist and Omniscan is lower than for the other four. The iron concentration in the supernatants (red), determined by a thiocyanate test, reveals a higher iron concentration in the supernatants for the CAs Gadovist and Omniscan than for the other four CAs.

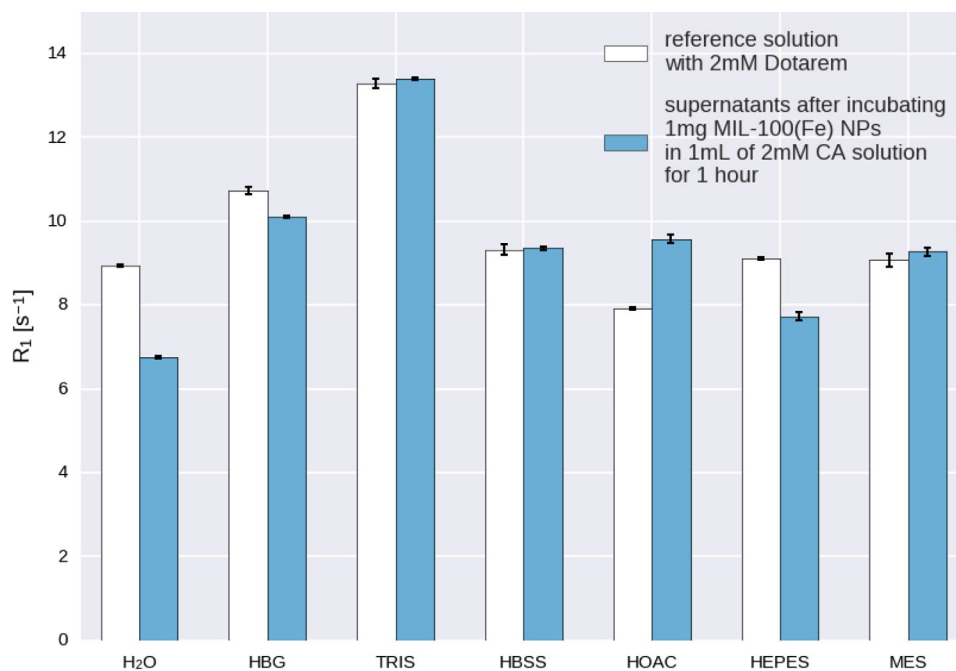


Figure 3. R_1 relaxation rates of supernatant solution after loading of Dotarem to MIL-100(Fe) in water and in 6 different buffers (blue). The same loading procedure was used as for sample preparation of Figure 1. Additionally, reference samples containing the specific solvent with 2 mM Dotarem were prepared and analyzed (white). The error bars denote the standard deviation of the R_1 relaxation rates for each sample. The corresponding R_2 relaxation rates are shown in Figure S7, Supporting Information.

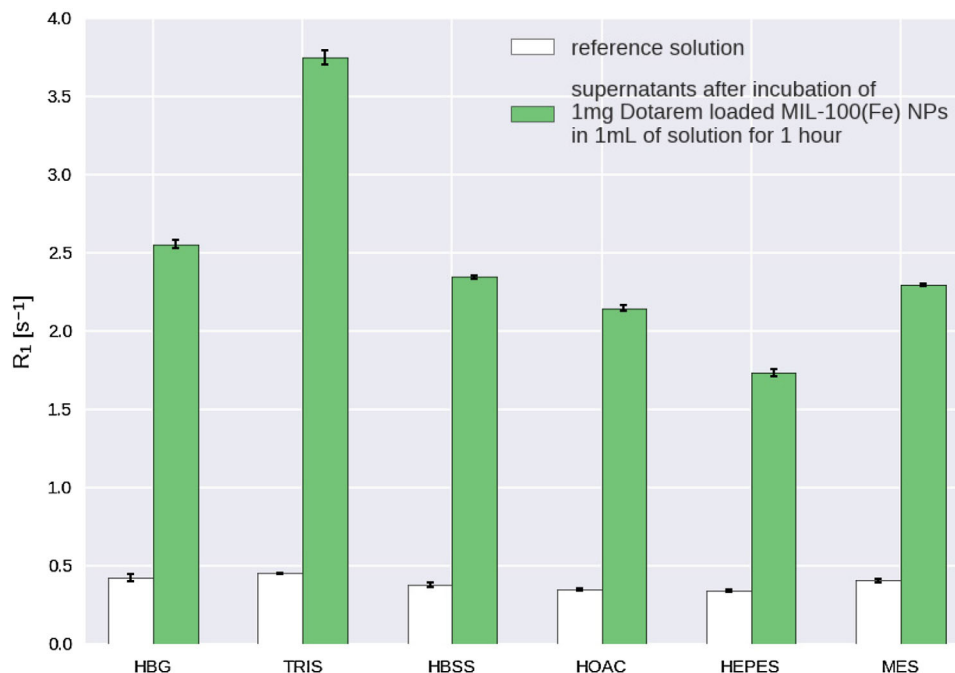


Figure 4. MRI investigation of CA release from NPs in diverse buffers. R_1 relaxation rates of supernatant solutions (green) of 1 mg MIL-100(Fe) previously loaded in H_2O with a concentration of 2 mM Dotarem. The loaded NPs were exposed for 1 h to six different buffers before removal and MRI analysis of the supernatants. For comparison, corresponding buffer solutions without CA (white) were also examined. The error bars denote the standard deviation of the R_1 relaxation rates for each sample. The corresponding R_2 relaxation rates are displayed in Figure S8, Supporting Information.

cells (late endosomes or lysosomes), HOAc buffer was applied. Additionally, Hank's balanced salt solution (HBSS) and HBG as an osmotically balanced equivalent of HEPES (20 mM, containing 5 mM glucose), were used because of their known physiological properties for biomedical applications.

Similar to the preceding experiments using different CAs, a decreased R_1 or R_2 in the supernatants in comparison to the corresponding reference solution was considered indicative for successful loading of the CA to the NPs. This was only seen using water and HEPES. Using the other buffers, no loading or again additional competing MRI signal forming processes were detected. Due to the known stability of the NPs^[11] in water together with the simplified use and availability, water was chosen as the medium for all further loading procedures reported here.

2.3. Testing CA Release of Dotarem in Diverse Buffers

Release of Dotarem from NPs loaded in aqueous CA solution was investigated in six different buffers (see Figure 4 and Figure S8, Supporting Information). The different solutions were used to investigate how sensitive the release is to modified chemical environments and whether one of these is more effective for testing. The same amount of NPs loaded with CA were redispersed and left for 1 h before centrifugation and characterization of the gained supernatants by MRI. A successful release of CA was expected to show increased relaxation rates in supernatants when compared to the corresponding reference solution (without

exposition to loaded NPs). All supernatants of the diverse buffers showed an increase in R_1 and R_2 which was the first indication that CA is released and will be further analyzed in the following sections using HBG.

HBG is a commonly used standard buffer for in vivo applications. For this reason, HBG was chosen for further testing and for proving principle in the following experiments. The other buffers were not excluded in general and thus could also be used for the following investigations.

2.4. Precision of MRI Methods and CA Concentration Assessment

After showing successful Dotarem loading in water and the first experiments investigating release, the precision of the MRI methods was tested. At first, R_1 and R_2 measurements were carried out for eight different concentrations of Dotarem in water and HBG, using two separately produced samples per concentration, that is, 16 samples per solution (see Figures S9 and S10, Supporting Information). In each case, a linear fit was performed and each of these resulting fit lines was then used as a calibration curve to calculate the amount of Dotarem in five control samples per solution (see Figures S11, S12, S13, and S14, Supporting Information). Additionally, each control sample was measured by ICP-AES as a control for the MR results.

The MRI results of each sample used for the calibration lines show a low standard deviation; the error bars in Figures S9 and S10, Supporting Information, are in fact smaller than the

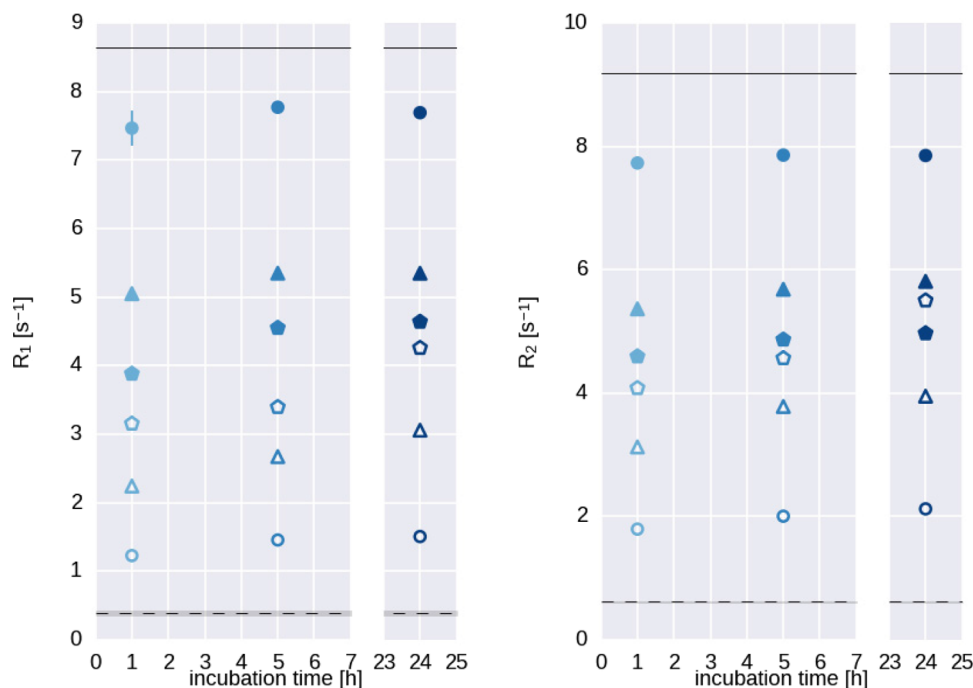


Figure 5. CA loading of NPs in H₂O. Figures show relaxation rates R_1 and R_2 of supernatants after loading procedures and subsequent centrifugation of three different amounts of loaded NPs. 1 mg (circles), 3 mg (triangles), and 5 mg (pentagons) of MIL-100(Fe) NPs were loaded either in a 2 mM aqueous Dotarem solution (filled symbols) or, for reference, in water only (empty symbols). The solid black lines and the dashed lines show the R_1 or R_2 of a 2 mM aqueous Dotarem reference solution or of H₂O, respectively. Standard deviations for the R_1 and R_2 results were determined and the only visible error bar is shown for the R_1 result of the 1 mg sample loaded in 2 mM aqueous Dotarem solution. All other error bars are not displayed, as they were within the boundaries of the markers (i.e., below 0.096 s⁻¹ for R_1 results and below 0.057 s⁻¹ for R_2 results)

markers for most of the measurements. The results of the separate sample sets (marked as sample set 1 and 2 in Figures S9 and S10, Supporting Information) are considered equal as demonstrated by the figures and showing that the sample production as well as the MRI measurements are very consistent.

The concentrations of the control samples calculated via MRI measurements (see Figures S11–S14, Supporting Information) match the intended concentrations and the concentration determined by ICP-AES precisely, that is, less than 0.1 mM deviation from the intended concentration in all but two cases for the calibration in H₂O and one for the calibration in HBG. In those cases, the deviation was below 0.3 mM.

The slopes of the lines for R_1 and R_2 shown in Figures S9 and S10, Supporting Information, are called the relaxivities r_1 and r_2 , respectively. Relaxivities indicate the contrast changing effectiveness of a CA in the solution.

Relaxivities for Dotarem in water were reported by several authors in literature. Laurent et al. reported an r_1 of 3.1 s⁻¹mm⁻¹ at 1.41 T,^[5] Rohrer et al. state an r_1 of 2.7 to 3.1 s⁻¹mm⁻¹, and an r_2 of 2.5 to 3.9 s⁻¹mm⁻¹ at 1.5 T and 37 °C^[5] and Aime et al. state an r_1 of 3.6 s⁻¹mm⁻¹ and an r_2 of 4.3 s⁻¹mm⁻¹ at 1.5 T and 37 °C.^[16] Considering potential differences of experimental conditions, that is, temperature, calculation, or imaging methods, the results shown here (r_1 and r_2 of 4.0 s⁻¹mm⁻¹, Figures S9 and S10, Supporting Information) were regarded as valid and in accordance with literature. These results were also regarded as verification of the MRI and calculation methods applied in this study.

2.5. Effect of Time and Amounts of NPs on the Loading Process

This section covers the question whether the amount of CA loaded to MIL-100(Fe) NPs can be further modified by increasing the loading time periods and by varying the NP amount. The previously shown loading procedures were all carried out for 1 h.

Figure 5 shows MRI results investigating the loading process in water with different amounts of NPs and different incubation times. A total of 18 loading processes were carried out in 2 mM aqueous Dotarem solution (1 mL) using three different amounts of NPs (1, 3, and 5 mg). For each of these amounts, samples were exposed to buffers for three different time periods before NPs were removed by centrifugation. As a control, samples were prepared performing exactly the same loading process but without adding CA. The NPs created in these mock loading procedures will further on be called “empty” NPs. The supernatants acquired after these loading processes were also analyzed in MRI.

Increasing the NP amount present during loading, resulted in decreasing relaxation rates (Figure 5), which is consistent with an increased CA uptake by NPs. Results from supernatants of loaded and “empty” NPs were clearly separated.

The MRI results for the supernatants of loaded and “empty” NPs seemed to converge only for the highest NP amount of 5 mg in R_1 or even to overlap in R_2 indicating that most of the CA present during loading is taken up by the NPs.

At the same time, the increasing relaxation rates of supernatants with increasing amount of “empty” NPs indicate that either the NPs cannot fully be removed during centrifugation or

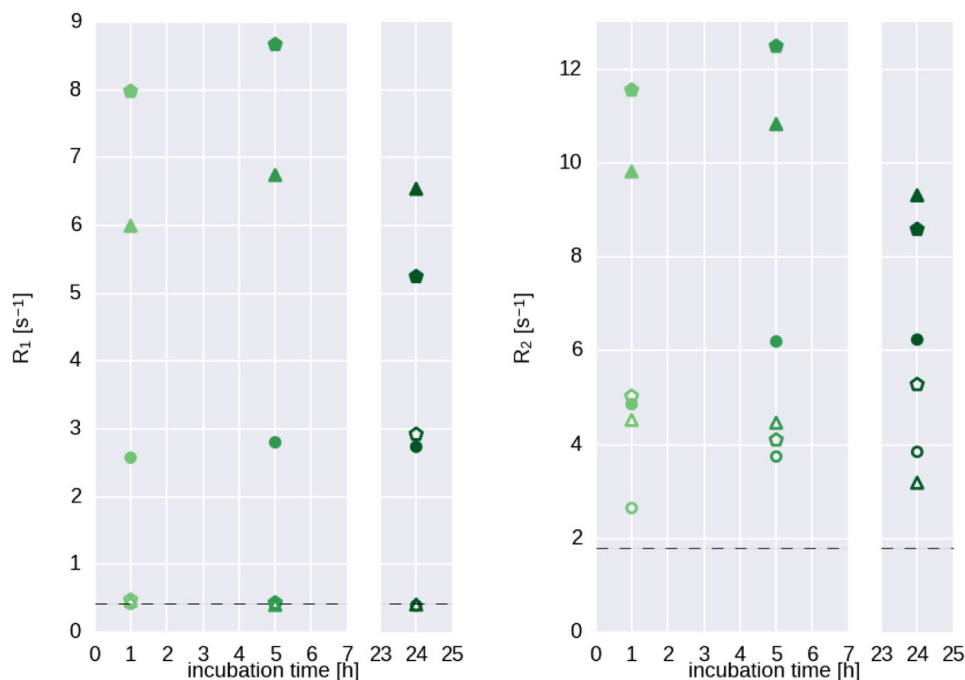


Figure 6. Dotarem release from MIL-100(Fe) NPs in HBG. Plots show relaxation rates R_1 and R_2 of supernatants after release was stopped by removal of the NPs. In preparations of these experiments, NPs were loaded either in a 2 mM Dotarem aqueous solution (filled symbols) or, for reference, in water only (empty symbols) for 1 h. 1 mg (circles), 3 mg (triangles), and 5 mg (pentagons) of these NPs were re-immersed in HBG for investigation of content release. Standard deviations for the R_1 and R_2 results were determined but not displayed, as they are all within the boundaries of the markers (i.e., below 0.051 s^{-1} for R_1 results and below 0.11 s^{-1} for R_2 results)

that residual NP components are present after partial or even full disintegration of the NPs. A disintegration of NPs after certain time periods in water is not a fundamental problem and even desirable as NPs should be extractable from the body in clinical use after a certain time. This has to be taken into account when analyzing MRI results of loading procedures.

Loading processes with CA and time periods of more than 1 h showed only minor increases of relaxation rates, which indicates that most of the CA is already taken up within the first hour. This outcome is a favorable result as it allows time savings when preparing labelled NPs.

2.6. Effect of Time and Amounts of NPs on the Release Process

The release process in HBG was investigated in a similar manner as described for the loading procedure. At first MIL-100(Fe) NPs were incubated in 2 mM aqueous Dotarem solution and extracted after centrifugation. Release processes with three different amounts of NPs (1, 3, and 5 mg) and three different incubation times (1, 5, 24 h) for each of these amounts were then carried out by incubating the NPs in HBG and removing them after the specified incubation time. Mock release processes with the same parameters were also carried out by using “empty” NPs, that is, NPs that were previously incubated in water only.

Supernatants, originating from CA loaded NPs, showed a trend toward increasing relaxation rates between 1 and 5 h and also increasing relaxation rates with an increase of the

NPs—the higher the amount, the more CA was released into the solution (see filled markers in Figure 6). Increasing relaxation rates in supernatants again implied higher CA content or preceding CA release from NPs, respectively. After 24 h relaxation rates seemed stable or starting to decrease again. Most of the CA release seemed to happen within the first hour.

The relaxation rates determined for supernatants from “empty” NPs (see empty markers in Figure 6) confirmed that the relaxation rate changes were related to CA release. These results show almost no dependency on R_1 and were comparable to the R_1 of HBG. This was different for R_2 with increased relaxation rates of supernatants from “empty” NPs relative to R_2 of HBG. These results did not show a clear trend between different amounts of NPs indicating that some residuals are still present which may be less compared to those of Figure 5.

The sample marked by the empty pentagon at 24 h in Figure 6 supposedly contained 5 mg of “empty” NPs but showed unexpected relaxation rates that would indicate the presence of Dotarem CA. Due to an unintended mislabeling, this sample was retrospectively identified by ICP-AES as being produced not from “empty” NPs but from CA loaded NPs instead (see next section).

CA is clearly released when loaded NPs were re-immersed in HBG and increasing amounts of loaded NPs showed increased CA release as expected. 1 h seemed sufficient to release most of the CA. Increased R_2 relaxation rates originating from “empty” NPs showed that some residuals of NPs besides CA are present in the supernatants. Results of supernatants from “empty” NPs did not markedly change although the incubation time during release and the amounts of NPs were varied. Considering the

observation that results from loaded NPs were separable from those of “empty” NPs—especially when larger amounts of NPs were used—this kind of experiments allows for a detailed investigation of CA release from NPs. It is recommended to add similar reference samples in future experiments to assess such additional signal forming processes besides those originating from CA loading and release. The presence and assessment of two MR-active components in a sample is addressed in the next experiments.

2.7. Assessing and Verifying Concentration of Two MR-Active Components by MRI

The presence of two different MR-active components may be a major challenge because both affect the MRI signal similarly. For instance, Gd and Fe will both shorten relaxation times with increasing concentration. If both are present at the same time in a solution, a simple determination of R_1 and R_2 in a macroscopic voxel will typically not allow for a differentiation of the two individual contributions to signal change. This is a common problem in MRI because the CA or MR-active components are not directly visualized by MRI but instead CAs are indirectly visible by changing the relaxation rates of the signal-giving water protons in their near vicinity.^[6] This challenge already led to the use of supernatants in MRI experiments where mainly one CA, namely Dotarem, was expected in the supernatants. The preceding results have shown that both, iron-containing contributions of MIL-100(Fe) NPs and the CA Dotarem, may be present in the supernatants at same time even after careful removal of NPs by centrifugation. Thus, it seemed very necessary to find an MRI method allowing the separate identification of two different MR-active components without the use of additional non-MRI methods.

Under certain conditions, when analyzing a solution that contains two known CAs, it is possible to retrieve the concentrations of both CAs by an MRI method introduced as “dual-contrast – magnetic resonance fingerprinting” (DC-MRF).^[17] *A priori* information for each of the two CAs/MR-active components are required as a prerequisite for this method to work. The R_1 and R_2 values for the CA mixture of interest, as well as for the base solution without any CAs, have to be determined. Furthermore, r_1 and r_2 values for each of the two CAs have to be determined separately in the base solution of interest. Using this information, the concentration of both CAs may be calculated as described by Anderson et al.^[17] The feasibility of this method for the characterization of the supernatants was tested here.

The solutions of interest consist of Gd-based CA and Fe-based NP components acting as a CA. The clinically approved Gd-CA Dotarem is already well known and relaxivities may be determined easily by varying the amount of CA in the solution and performing appropriate MR experiments on those solutions. In contrast to this, the exact nature of the MR-active components of MIL-100(Fe) remaining in the supernatant after centrifugation is unknown. For example, leftover NPs after centrifugation could affect the MRI results differently when compared to iron ions or debris of the NPs. Because of this and the yet not well known dynamics, the calibration curves for the “second” CA are hardly assessable beforehand for a specific supernatant containing a mix-

ture of Fe ions, intact NPs or debris of MIL-100(Fe). Here, as a surrogate, calibration curves have been determined based on samples where different amounts of NPs were incubated in either water or HBG without adding CA. These “empty” NPs were removed by centrifugation after 1 h with subsequent MRI measurements of the supernatants (see Figures S15 and S16, Supporting Information). Additionally to MRI, the concentration of iron and gadolinium ions present in the supernatants was also determined using ICP-AES. Calibration curves for Dotarem have already been acquired to determine the precision of this method (see Figures S9 and S10, Supporting Information). Using these calibration curves and applying the DC-MRF-method, the iron and gadolinium concentration of the 5- and 24-h samples seen in Figures 5 and 6 were assessed and compared to the ICP-AES results.

Figures 7 and 8 show the concentrations of Fe- and Gd-based on MRI measurements in comparison to the concentrations obtained via ICP-AES for the experiments investigating 5-h CA loading in water and CA release in HBG, respectively. The corresponding results for the 24 h loading and release experiments are presented in Figures S17 and S18, Supporting Information. For the loading experiments (Figure 7 and Figure S17, Supporting Information), the gadolinium concentrations assessed by MRI were in good accordance with ICP-AES. On average, the iron content is overestimated by 0.6 mM with a standard deviation of about 0.2 mM (see Figure 7 and Figure S17, Supporting Information). This is also true for the CA release process in HBG with the difference that assessment seems more precise and more accurate (Figure 8). The iron content was overestimated by about 0.3 mM with a standard deviation of about 0.3 mM. The gadolinium content was, on average, underestimated by less than 0.1 mM with a standard deviation of about 0.1 mM.

The surrogate calibration curves for iron are made from “empty” NPs which means that potential residual fragments of loaded NPs are neglected. Furthermore, ICP-AES is “only” counting Fe- and Gd-ions whereas in MRI the signal will be affected differently depending on the chemical nature. This means that two samples containing the same amount of iron but with different chemical nature may result in different relaxation times. Calibration curves for clinically approved Gd-based CA do not suffer from such problems as each CA-molecule contains only one Gd-atom. These could be the reasons for overestimating iron concentration using DC-MRF.

Applying the DC-MRF method to supernatants investigating “CA release” from “empty” NPs, ideally no Gd-content should be found (empty green markers in Figure 7 and Figure S17, Supporting Information). Instead the method minimally underestimates the gadolinium content and overestimates the iron content (empty brown/orange markers in Figure 7 and Figure S17, Supporting Information). One explanation for this observation is that the DC-MRF method is highly effective if r_1 and r_2 of the CAs calibration curves are sufficiently different. In the experiments here, the calibration curves of Dotarem and the MIL-100(Fe) residuals in water were similar. For Dotarem in water, r_1 and r_2 were both $4.0 \text{ s}^{-1} \text{ mM}^{-1}$ (Figure S9, Supporting Information) and for the residuals the values for r_1 and r_2 were very similar, that is, 2.9 and $2.0 \text{ s}^{-1} \text{ mM}^{-1}$ (Figure S15, Supporting Information), respectively. In HBG, the r_1 and r_2 of Dotarem were both $5.0 \text{ s}^{-1} \text{ mM}^{-1}$ (Figure S7, Supporting Information) but very different for the

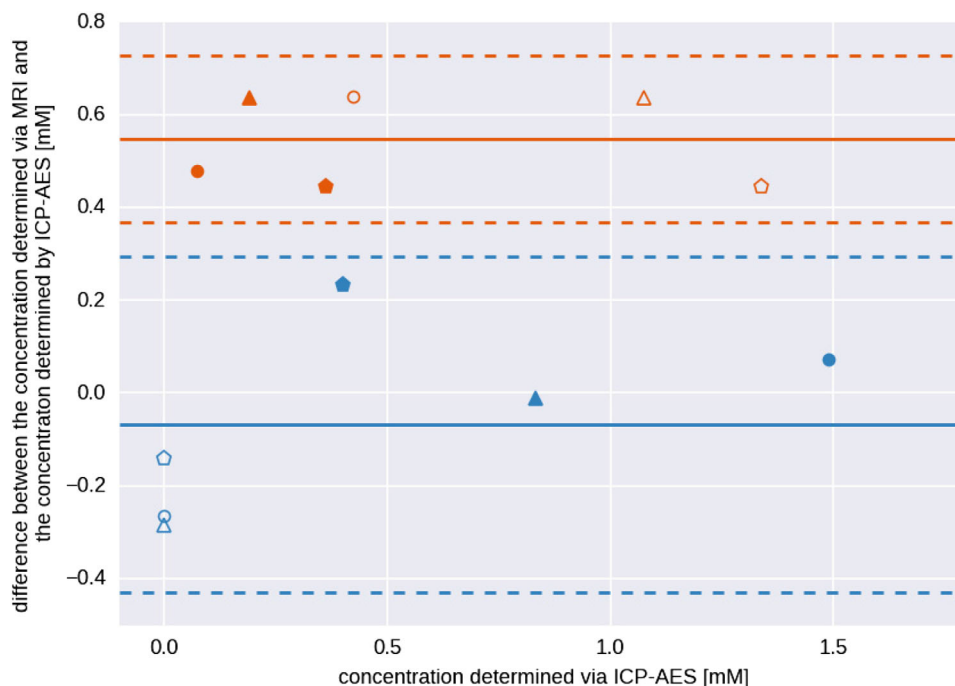


Figure 7. Bland–Altman plot for the supernatants after the 5-h loading procedures in H₂O. The samples used in Figure 5 were analyzed using the “dual-contrast MRI fingerprinting” method. Blue markers indicate the gadolinium and orange markers indicate the iron content. 1 mg (circles), 3 mg (triangles), and 5 mg (pentagons) of MIL-100(Fe) NPs were loaded either in a 2 mM aqueous Dotarem solution (filled symbols) or, for reference, in water only (empty symbols). ICP-AES was the gold standard.

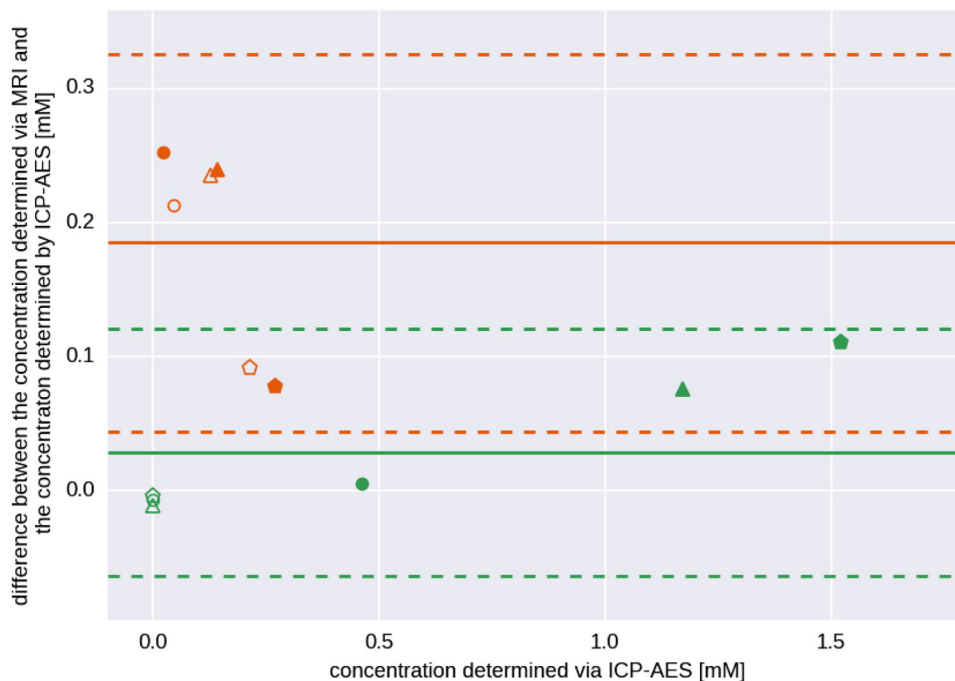


Figure 8. Bland–Altman plot for the supernatants after the 5-h release procedures in HBG. The samples used in Figure 6 were analyzed using the “dual-contrast MRI fingerprinting” method. Green markers indicate the gadolinium and orange markers indicate the iron content. NPs were loaded either in a 2 mM Dotarem aqueous solution (filled symbols) or, for reference, in water only (empty symbols) for 1 h and were removed afterwards. 1 mg (circles), 3 mg (triangles), and 5 mg (pentagons) of these NPs were re-immersed in HBG for investigation of content release. ICP-AES was the gold standard.

residuals, that is, 0.1 and 7 s⁻¹ mM⁻¹ (Figure S16, Supporting Information), respectively. There is also a clear difference between the iron content of the samples loaded in 2 mm aqueous Dotarem solution (filled markers) and the ones loaded in water only (empty markers) (Figure 7 and Figure S17, Supporting Information). The supernatants prepared from loaded NPs contain less iron than those prepared from “empty” NPs. MIL-100(Fe) NPs with Dotarem attached to them are heavier than the “empty” NPs and their removal via a centrifuge may be more effective. This suggests that the MIL-100(Fe) residuals consist mostly of NPs and not of ions from decomposed NPs. In Figure S13, Supporting Information, this seems even more pronounced as based on ICP-AES results, iron content was very low for the 24 h release experiments in HBG disregarding whether supernatants of loaded or “empty” NPs were interpreted. One explanation could be that NPs in HBG tend to agglomerate at long time periods disregarding the presence of CA and thus NPs or residuals are more effectively removed from supernatants by centrifugation.

DC-MRF was successfully used in this study to differentiate between the residuals of NPs and CA in the supernatants. While the CA concentration was accurately determined, Fe concentrations were overestimated. With further understanding of the nature of the MIL-100(Fe) residuals, it should be possible to create more precise calibration curves and further improve the analysis.

3. Conclusion

In this work, six clinically approved and unmodified MRI CAs were systematically tested as an imaging label for the porous NPs MIL-100(Fe). Dotarem was identified as the best CA for labelling MIL-100(Fe) NPs enabling MRI visualization of loading and release. More detailed investigations of the loading and release processes, including precision tests of the utilized MRI methods, were carried out.

Results were thoroughly tested by independently prepared sample batches and repeated experiments. Additionally, MRI results were verified by ICP-AES and thiocyanate-based determination of gadolinium and iron concentrations. Performed in a clinical MRI system at 1.5 T, the applied MRI methods for R_1 and R_2 determination were shown to be suitable for the systematic research of CA loading and release processes. Both processes were shown to happen within the first hour and to be strongly dependent on the used buffer. Using a clinical MRI setting and clinically approved MRI CAs for labeling porous NPs and in a next step the nanocarrier system facilitates the translation of results to clinical application. Based on the results of this study the authors think that the presented methodology can serve as a blueprint for investigating other promising porous NPs foreseen for MRI visualization of loading and release processes based on CAs.

MIL-100(Fe) and of course MRI-CAs are both MR-active, affecting the MRI signal by comparable mechanisms. To allow investigation of CA loading and release processes, supernatants were analyzed assuming that after centrifugation of NPs only CA will be the dominating MR-active component. In the course of this study, it has been shown that besides the expected CA content also residuals of the iron-based MOF NPs were present after thorough removal of NPs. This indicates that additional processes besides CA loading and release from MIL-100(Fe) have

to be considered in future research. In that case two MR-active components in a solution are present and to allow differentiation the “dual-contrast MRI fingerprinting” method was adapted and tested successfully. Concentrations of Dotarem and MOF residuals in supernatants were shown to be assessable. The application of this method allows a first interpretation of MRI results originating from CA loading or release to MR-active NP nanocarrier systems without the need of additional methods such as ICP-AES.

Labeling of NPs for MRI visualization is typically performed to trace the NPs and their accumulation in a tissue of interest. The demonstrated feasibility of NP-loading with clinically approved CAs adds a new concept of labeling MOF NPs for MRI visualization that has not been investigated in a systematic way before. Furthermore, successful loading and release of MOF NPs with an MRI-CA creates a basis for new theranostic MOF NPs as visualization of release of CA from NPs which may be related to release of co-loaded drugs and their biodistribution. The feasibility of such concepts has been shown for liposomes already.^[6]

The results found in this study justify further research using Dotarem (one of the most future-proof CAs) as an imaging label for the most promising biocompatible MOF NP candidate MIL-100(Fe) with the aim to develop a drug-delivery system allowing characterization of loading and release. Co-loading of CAs and therapeutic drugs to NPs MIL-100(Fe) seems to be the next step in future research.

4. Experimental Section

MRI Measurements: All MR measurements were performed in a clinical setting using a Siemens MAGNETOM Aera 1.5T MRI scanner (Siemens Healthineers, Erlangen, Germany) with a standard head coil. Samples were filled into 2 mL Eppendorf-tubes for MRI. An ensemble of up to 24 samples was fixed in a dedicated PMMA holder and submerged in a water bath (Figure 9). The bath containing the samples was then fixed in the head coil. The MRI measurements were performed at room temperature.

The MRI analysis in this work was based on the determination of relaxation times T_1 [s] and T_2 [s] of supernatant samples under different experimental conditions.

For T_1 determination a set of images was acquired using a saturation-recovery pulse sequence with 30 recovery times between 130 and 5000 ms and an accordingly adapted TR between 300 and 5150 ms. The other parameter settings were: TE 1.71 ms, matrix 128*128, FOV 126 mm*126 mm and slice thickness 6 mm. For each of the 30 recovery times in total 15 experiments were performed. Always five images for a specific recovery time of these 15 were averaged. This resulted in three sets consisting of 30 averaged images with varying saturation times. T_1 values were determined for each set as described below and the mean and standard deviation of these T_1 values are displayed as relaxation rates R_1 in Figures 3–6, Figures S9, S10, S15, and S16, Supporting Information.

For the T_2 determination a set of images was created with a multi-echo sequence that was applied twice with two different sets of 16 echo times that were either in the range 15–240 or 50–800 ms, respectively. Each set consisted therefore of 16 images. All other parameters were kept constant: TR 3000 ms, three averages, matrix 256*256, FOV 126 mm*126 mm and slice thickness 6 mm). The former set of TEs was used for solutions with a high R_2 and the latter for solutions with lower R_2 .

Both multi-echo sequence sets were repeated three times allowing to calculate correspondingly three T_2 values for each sample as described below. The mean and standard deviation of the corresponding three

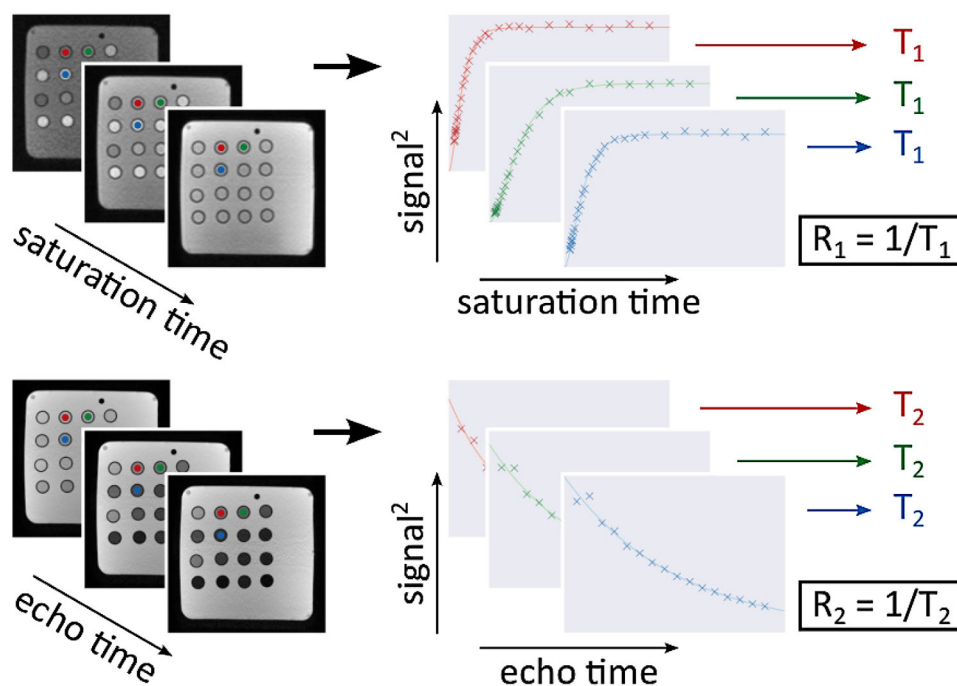


Figure 9. Simplified image processing pipeline. In a MRI experiment a set of samples filled in Eppendorf tubes was simultaneously investigated as demonstrated by the MRI images on the left (three exemplary images of the 16 samples shown here). For each sample set always two sets of images were recorded using varying saturation times to determine T_1 relaxation times (top row), and varying echo times to determine T_2 relaxation times (bottom row). The two displayed MRI images sets show the same cross section of the Eppendorf tubes containing the samples immersed in a water bath. A region of interest was selected for each sample to extract the mean signal evolution over saturation or echo time for that specific sample (here three samples are marked by colors for demonstration). Finally, a fit (solid lines) of the squares of the extracted signals (marked with crosses), using the appropriate squared exponential functions, was used to determine the different T_1 and T_2 relaxation times and the corresponding relaxation rates of a specific sample.

relaxation rates R_2 values are displayed in Figures 5 and 6, S7–10, S15, and S16, Supporting Information.

Image analysis and calculation of T_1 and T_2 values was performed using in-house developed software based on Python (Python Software Foundation, Python Language Reference, available at <http://www.python.org>). Regions of interest were selected for each sample to determine the average of the signal of this sample (a simplified scheme of this procedure is shown in Figure 9). The squared signal averages of a sample were plotted against the corresponding recovery times and echo times for T_1 and T_2 determination (Figure 9), respectively. For each relaxation time and each sample a subsequent noise corrected fit was performed on the squares of the averages using a Levenberg–Marquardt algorithm according to Raya et al.^[18]

The graphs in Figures S9, S10, S15, and S16, Supporting Information, show the relaxation rates R_1 and R_2 ($R_i = 1/T_i$, $i = 1, 2$) of the samples in relation to CA concentration. For clinically approved CAs, R_i values increase linearly with increasing concentration of CA under the conditions used,^[9] where the slopes represent the relaxivities r_i [$s^{-1} \text{ mm}^{-1}$] ($i = 1, 2$). These are determined by a linear fit as displayed in Figures S9, S10, S15, and S16, Supporting Information). The linear fit in this work was performed using a Levenberg–Marquardt algorithm.

Inductively Coupled Plasma Atomic Emission Spectrometry: In this work, ICP-AES was used either to assess the composition of NP pellets or the content of supernatants after a loading or release process. The detailed preparation of the specific samples is described in the supporting information for each case. Dried NP pellets were digested in 69% (v/v) HNO_3 for trace analysis and subsequently diluted with bi-distilled water to 3% (v/v) HNO_3 . The samples were then analyzed for their gadolinium and iron content by ICP-AES (CCD simultaneous ICP-AES Vista RL, Agilent, Santa Clara, USA). The wavelengths 335048 and 342246 nm used for gadolinium and the wavelengths 259940 and 239563 nm were used for iron. The

results from these measurements are reported here without standard deviation as it was too low to display.

Determination of Iron Content by UV–Vis (Thiocyanate/Rhodanide Method):

Calibration: The iron content of the supernatant after incubation of MIL-100(Fe) NPs in different CA solutions was determined by UV–vis spectroscopy, measuring the absorption of the blood-red iron thiocyanate complex, which is formed by combining thiocyanate and Fe(III) ions in solutions.

A calibration curve was determined by preparing different $\text{FeCl}_3 \cdot 6 \text{H}_2\text{O}$ solutions with concentrations 0.02, 0.05, 0.1, 0.2, 0.5, and 1 mM (see Figures S19 and S20, Supporting Information). An excess of ammonium thiocyanate (1 μL , 1 M in H_2O) was added to 20 μL of iron ion solution and after 5 min, UV–vis absorption in the maximum region (480 and 483 nm) was recorded by a NanoDrop 2000 spectrometer (Thermo Fisher Scientific, Waltham, USA). Based on this data, the equation of the two linear calibration curves (480 and 483 nm) was determined and applied for the calculation of the amount of iron content in the MIL-100(Fe) + CA supernatant.

Iron Amount of Supernatants: After incubation of the 1 mg MIL-100(Fe) NPs in the CA solution for 1 h, the MOF NPs were centrifuged and 20 μL of the supernatant were spiked with 1 μL of ammonium thiocyanate solution (1 M). After 5 min, the UV–vis absorption of the solution was measured at 480 and 483 nm and the iron content was calculated as the average of both measurements based on the previous calibrations.

Supporting Information

Supporting Information is available from the Wiley Online Library or from the author.

Acknowledgements

The authors are grateful for financial support from the Deutsche Forschungsgemeinschaft (DFG) through DFG-project WU 622/4-1 and PE 925/3-1, the Excellence Cluster Nanosystems Initiative Munich (NIM) and the Center for NanoScience Munich (CeNS).

Conflict of Interest

The authors declare no conflict of interest.

Keywords

drug delivery systems, loading and release, MOFs, MRI, porous nanoparticles

Received: July 1, 2019

Revised: August 29, 2019

Published online: October 15, 2019

- [1] a) S. S. Kelkar, T. M. Reineke, *Bioconjugate Chem.* **2011**, *22*, 1879; b) J. H. Ryu, S. Lee, S. Son, S. H. Kim, J. F. Leary, K. Choi, I. C. Kwon, *J. Controlled Release* **2014**, *190*, 477; c) B. Pelaz, C. Alexiou, R. A. Alvarez-Puebla, F. Alves, A. M. Andrews, S. Ashraf, L. P. Balogh, L. Ballerini, A. Bestetti, C. Brendel, S. Bosi, M. Carril, W. C. Chan, C. Chen, X. Chen, Z. Cheng, D. Cui, J. Du, C. Dullin, A. Escudero, N. Feliu, M. Gao, M. George, Y. Gogotsi, A. Grunweller, Z. Gu, N. J. Halas, N. Hampp, R. K. Hartmann, M. C. Hersam et al., *ACS Nano* **2017**, *11*, 2313. PMID: 28290206.
- [2] M. W. Dewhirst, T. W. Secomb, *Nat. Rev. Cancer* **2017**, *17*, 738.
- [3] A. A. Manzoor, L. H. Lindner, C. D. Landon, J. Y. Park, A. J. Simnick, M. R. Dreher, S. Das, G. Hanna, W. Park, A. Chilkoti, G. A. Koning, T. L. ten Hagen, D. Needham, M. W. Dewhirst, *Cancer Res.* **2012**, *72*, 5566.
- [4] a) Y. H. Yun, B. K. Lee, K. Park, *J. Controlled Release* **2015**, *219*, 2; PMID: 26456749. b) T. Lammers, F. Kiessling, W. E. Hennink, G. Storm, *J. Controlled Release* **2012**, *161*, 175; c) C. M. Dawidczyk, C. Kim, J. H. Park, L. M. Russell, K. H. Lee, M. G. Pomper, P. C. Searson, *J. Controlled Release* **2014**, *187*, 133.
- [5] a) S. Laurent, L. V. Elst, R. N. Muller, *Contrast Media Mol. Imaging* **2006**, *1*, 128; b) M. Rohrer, H. Bauer, J. Mintorovitch, M. Requardt, H. J. Weinmann, *Invest. Radiol.* **2005**, *40*, 715; c) A. J. Villaraza, A. Bumb, M. W. Brechbiel, *Chem. Rev.* **2010**, *110*, 2921; d) G. B. Chavhan, P. S. Babyn, B. Thomas, M. M. Shroff, E. M. Haacke, *Radio Graphics* **2009**, *29*, 1433.
- [6] a) M. Peller, L. Willerding, S. Limmer, M. Hossann, O. Dietrich, M. Ingris, R. Sroka, L. H. Lindner, *J. Controlled Release* **2016**, *237*, 138; b) A. M. Ponce, B. L. Viglianti, D. Yu, P. S. Yarmolenko, C. R. Michelich, J. Woo, M. B. Bally, M. W. Dewhirst, *J. National Cancer Inst.* **2007**, *99*, 53; c) M. de Smet, E. Heijman, S. Langereis, N. M. Hijnen, H. Grull, *J. Controlled Release* **2011**, *150*, 102; d) B. L. Viglianti, A. M. Ponce, C. R. Michelich, D. Yu, S. A. Abraham, L. Sanders, P. S. Yarmolenko, T. Schroeder, J. R. MacFall, D. P. Barboriak, O. M. Colvin, M. B. Bally, M. W. Dewhirst, *Magn. Reson. Med.* **2006**, *56*, 1011.
- [7] R. Freund, U. Lachelt, T. Gruber, B. Ruhle, S. Wuttke, *ACS Nano* **2018**, *12*, 2094. PMID: 29533060.
- [8] a) T. Simon-Yarza, A. Mielcarek, P. Couvreur, C. Serre, *Adv. Mater.* **2018**, *30*, e1707365; b) S. Wuttke, M. Lismont, A. Escudero, B. Rungtaweeworanit, W. J. Parak, *Biomaterials* **2017**, *123*, 172. PMID: 28182958.
- [9] a) P. Horcajada, T. Chalati, C. Serre, B. Gillet, C. Sebrie, T. Baati, J. F. Eubank, D. Heurtaux, P. Clayette, C. Kreuz, J. S. Chang, Y. K. Hwang, V. Marsaud, P. N. Bories, L. Cynober, S. Gil, G. Férey, P. Couvreur, R. Gref, *Nat. Mater.* **2010**, *9*, 172; b) T. Simon-Yarza, M. Gimenez-Marques, R. Mrimi, A. Mielcarek, R. Gref, P. Horcajada, C. Serre, P. Couvreur, *Angew. Chem., Int. Ed.* **2017**, *56*, 15565; c) J. Zhuang, C. H. Kuo, L. Y. Chou, D. Y. Liu, E. Weerapana, C. K. Tsung, *ACS Nano* **2014**, *8*, 2812; PMID: 24506773. d) B. Illes, S. Wuttke, H. Engelke, *Nanomaterials* **2017**, *7*, 351; e) C. He, K. Lu, D. Liu, W. Lin, *J. Am. Chem. Soc.* **2014**, *136*, 5181; f) R. Roder, T. Preiss, P. Hirschle, B. Steinborn, A. Zimpel, M. Hohn, J. O. Radler, T. Bein, E. Wagner, S. Wuttke, U. Lachelt, *J. Am. Chem. Soc.* **2017**, *139*, 2359; g) S. K. Alsaiani, S. Patil, M. Alyami, K. O. Alamoudi, F. A. Aleisa, J. S. Merzaban, M. Li, N. M. Khashab, *J. Am. Chem. Soc.* **2018**, *140*, 143; h) M. Lismont, L. Dreesen, S. Wuttke, *Adv. Funct. Mater.* **2017**, *27*, 1606314; i) Y. Chen, P. Li, J. A. Modica, R. J. Drout, O. K. Farha, *J. Am. Chem. Soc.* **2018**, *140*, 5678; PMID: 29641892. j) J. W. M. Osterrieth, D. Wright, H. Noh, C.-W. Kung, D. Vulpe, A. Li, J. E. Park, R. P. Van Duyne, P. Z. Moghadam, J. J. Baumberg, O. K. Farha, D. Fairen-Jimenez, *J. Am. Chem. Soc.* **2019**, *141*, 3893. PMID: 30707577.
- [10] S. Wuttke, A. Zimpel, T. Bein, S. Braig, K. Stoiber, A. Vollmar, D. Muller, K. Haastert-Talini, J. Schaeske, M. Stiesch, G. Zahn, A. Mohmeyer, P. Behrens, O. Eickelberg, D. A. Bolukbas, S. Meiners, *Adv. Healthcare Mater.* **2017**, *6*.
- [11] a) A. Zimpel, T. Preiß, R. Röder, H. Engelke, M. Ingris, M. Peller, J. O. Rädler, E. Wagner, T. Bein, U. Lächelt, S. Wuttke, *Chem. Mater.* **2016**, *28*, 3318; b) S. Wuttke, S. Braig, T. Preiss, A. Zimpel, J. Sicklinger, C. Bellomo, J. O. Radler, A. M. Vollmar, T. Bein, *Chem. Commun.* **2015**, *51*, 15752; c) T. Baati, N. Njim, F. Neffati, A. Kerkeni, M. Bouttemi, R. Gref, M. F. Najjar, A. Zakhama, P. Couvreur, C. Serre, P. Horcajada, *Chem. Sci.* **2013**, *4*, 1597.
- [12] V. M. Runge, J. T. Heverhagen, *Invest. Radiol.* **2018**, *53*, 381. PMID: 29462023.
- [13] E. M. Agency, <https://www.ema.europa.eu/en/medicines/human/referrals/gadolinium-containing-contrast-agents> **2019** (accessed: 2017).
- [14] M. Peller, K. Boll, A. Zimpel, S. Wuttke, *Inorg. Chem. Front.* **2018**, *5*, 1760.
- [15] A. García Márquez, A. Demessence, A. E. Platero-Prats, D. Heurtaux, P. Horcajada, C. Serre, J.-S. Chang, G. Férey, V. A. de la Peña-O'Shea, C. Boissière, D. Grosso, C. Sanchez, *Eur. J. Inorg. Chem.* **2012**, *2012*, 5165.
- [16] S. Aime, P. Caravan, *J. Magn. Resonance Imag.* **2009**, *30*, 1259.
- [17] C. E. Anderson, S. B. Donnola, Y. Jiang, J. Batesole, R. Darrah, M. L. Drumm, S. M. Brady-Kalnay, N. F. Steinmetz, X. Yu, M. A. Griswold, C. A. Flask, *Sci. Rep.* **2017**, *7*, 8431.
- [18] J. G. Raya, O. Dietrich, A. Horng, J. Weber, M. F. Reiser, C. Glaser, *Magn. Reson. Med.* **2010**, *63*, 181. PMID: 19859960.